Original Article

The application of backscattered ultrasound and photoacoustic signals for assessment of bone collagen and mineral contents

Bahman Lashkari[1], Lifeng Yang[1,2], Andreas Mandelis[1,2]

[1]Center for Advanced Diffusion-Wave Technologies (CADIFT), Department of Mechanical and Industrial Engineering, University of Toronto, Toronto, Ontario, Canada; [2]School of Optoelectronic Information, University of Electronic Science and Technology of China, Chengdu 610054, China

Correspondence to: Andreas Mandelis. Center for Advanced Diffusion-Wave Technologies (CADIFT), Department of Mechanical and Industrial Engineering, University of Toronto, 5 King's College Rd., M5S 3G8, Toronto, Ontario, Canada. Email: mandelis@mie.utoronto.ca.

Background: This study examines the backscattered ultrasound (US) and back-propagating photoacoustic (PA) signals from trabecular bones, and their variations with reduction in bone minerals and collagen content. While the collagen status is directly related to the strength of the bone, diagnosis of its condition using US remains a challenge.

Methods: For both PA and US methods, coded-excitation signals and matched filtering were utilized to provide high sensitivity of the detected signal. The optical source was a 805-nm CW laser and signals were detected employing a 2.2-MHz ultrasonic transducer. Bone decalcification and decollagenization were induced with mild ethylenediaminetetraacetic acid (EDTA) and sodium hypochlorite solutions, respectively.

Results: The PA and US signals were measured on cattle bones, and apparent integrated backscatter/back-propagating (AIB) parameters were compared before and after demineralization and decollagenization.

Conclusions: The results show that both PA and US are sensitive to mineral changes. In addition, PA is also sensitive to changes in the collagen content of the bone, but US is not significantly sensitive to these changes.

Keywords: Osteoporosis; ultrasonic backscattering; photoacoustic (PA); quantitative ultrasound (QUS); cancellous bone; collagen content; bone mineral density (BMD)

Submitted Sep 17, 2014. Accepted for publication Oct 10, 2014.
doi: 10.3978/j.issn.2223-4292.2014.11.11
View this article at: http://dx.doi.org/10.3978/j.issn.2223-4292.2014.11.11

Introduction

The complex architecture of bones and contribution of both organic and inorganic phases give rise to a very strong bio-structure. Traditionally, the fracture risk of bone has been mainly pursued as a result of decrease in bone mineral density (BMD). Clinical osteoporosis diagnostic modalities such as dual X-ray absorptiometry (DXA) can evaluate the BMD (1). Although BMD is definitely a major factor in the strength of bones, new studies suggest the chance of bone fracture even without BMD deficit (2-4). Bone minerals are responsible for compression strength of the bone and a vital factor for bone integrity. On the other hand, the organic phase of bones which is mainly collagen type I provides the bone with tensile strength and ductility due to its viscoelastic properties. The reduction of collagen content with aging (5-7) could be an important factor increasing fracture risk without decrease in bone minerals. The changes of collagen cross-links during osteoporosis have been the subject of several studies (4,8-10). There are still many unclear issues and more research is needed on the variation of the organic phase of bones with aging and as a result of diseases such as osteoporosis and diabetes. Therefore, any method or modality that can assess either the collagen content, or collagen cross-linking, or both, may assist in better understanding of bone diseases, their diagnosis and even the selection of therapeutic strategies. Some studies have proposed the assessment of collagen cross-linking by analyzing the urine or serum (7,8).

Responsive to mechanical properties and geometry of hard tissues, ultrasonic waves are proper candidates for delivering and revealing bone strength and microstructure. Ultrasonic evaluation of bones is not only useful for diagnosing osteoporosis, but can also yield a better understanding of biomechanical changes in the bone during the disease. The use of ultrasound (US) for diagnosis of osteoporosis started in the 1980s and essentially depends on the measurement of the speed of sound (SOS) and on normalized broadband ultrasonic attenuation (nBUA) (11-15). New approaches such as fast and slow wave detection and backscattered US were also introduced recently (15-17) and clinical instruments based on these parameters were proposed (16,18). Although they did not reduce the dominance of SOS and nBUA measurements in quantitative ultrasound (QUS), these alternative approaches introduce parameters that may reveal more information about the state of health of trabecular bones. The large number of mechanical parameters affecting the ultrasonic response, as well as the substantial variation of human bone tissue and complexity of its structure, are the major challenges of QUS in offering a reliable diagnostic method for osteoporosis. Nevertheless, the backscatter method has the advantage of facilitating measurements at crucial sites like hip or spine where the risk of fracture is high. Several parameters have been introduced and applied to quantify bone backscattered US. Some typical parameters are the frequency dependent backscatter coefficient [BSC or $\eta(f)$] (19-26), the apparent integrated backscatter (AIB) (27-31) and the broadband ultrasound backscatter (BUB) (32-35).

In this study, we measured both the US backscattering and also the photoacoustic (PA) back-propagating signal. The dependence of the PA signal on optical properties of the tissue provides more specific information about bone composition and structure. In our previous studies (36-39), it was shown that laser light can penetrate at least as deep as 1.5 mm in cortical bone and 3 mm in cancellous bone and can generate a detectable PA signal from those depths. It was shown that the PA back-propagating signal is sensitive to controlled changes of bone minerals. The PA signals also indicate the sensitivity to variation in bone composition. We could also detect a PA "coherent structure backscattering" in a way very similar to US in frequencies above 1 MHz. PA was also used to generate guided US waves in long bones for bone assessment (40,41).

The use of frequency-domain (FD) or CW US and PA is valuable for the spectral analysis of the signal which is essential in this study. The FD method is based on transmitting a broadband coded signal and using a matched filter at the receiving end to convert it to a time-domain depth-dependent signal trace. The use of coded-excitation in bone QUS has been investigated before in measurements of the BUA (42,43), slow and fast waves (44) and guided wave detection in long bones (45). FD-PA has been developed by our group (46-48) and has been used mainly for soft tissue imaging.

Materials and methods

The experimental set-up used for US and PA tests with two different laser wavelengths is depicted in *Figure 1A*. A pair of focused US transducers was employed for transmission and reception of continuous waves (3.5-MHz, model V382, and 2.2 MHz, model V305, Panametrics, Olympus NDT Inc., Waltham, MA, USA). Both transducers were wideband and had a focal length of 1. The transducers were chosen to have similar beam widths at half maximum which were estimated to be 0.87 and 0.9 mm for transmission and reception, respectively (49). Using the CW method, there was no need for RF power amplifier in the transmission line and the 2-V_{pp} voltage of the function generator produced adequate signal to noise ratio (SNR). However, for reception, a preAmp with 40 dB amplification was employed (5676 Panametrics, Olympus NDT Inc., Waltham, MA, USA). The bone sample and the transducers were immersed in a water container for acoustic coupling. To prevent the overlapping of regions of interest (ROIs) of A-scans used to calculate the ensemble average of the signal, 2-mm step sizes were used. Less than 50% of cross-sectional overlap is required to ensure independent signals (21).

Data acquisition and signal processing were performed in a PC using LabView software. Data acquisition was performed by an analog-to-digital convertor (ADC, PXIe-5122) and NI-SCOPE software (National Instruments, Austin, TX, USA). Waveform generation was performed by a digital-to-analog converter (DAC, NI PXI-5421) and NI-FGEN software (National Instruments, Austin, TX, USA). The two cards were synchronized using the internal clock of the instrument. The maximum sampling frequency of both cards was 100 MHz, which was used in all reported experiments.

The PA experiments were performed with the same system described above, except for the signal source which was a 805-nm CW diode-laser (Laser Light Solutions, Somerset, NJ, USA), with a driver which was controlled by a software function generator to modulate the laser

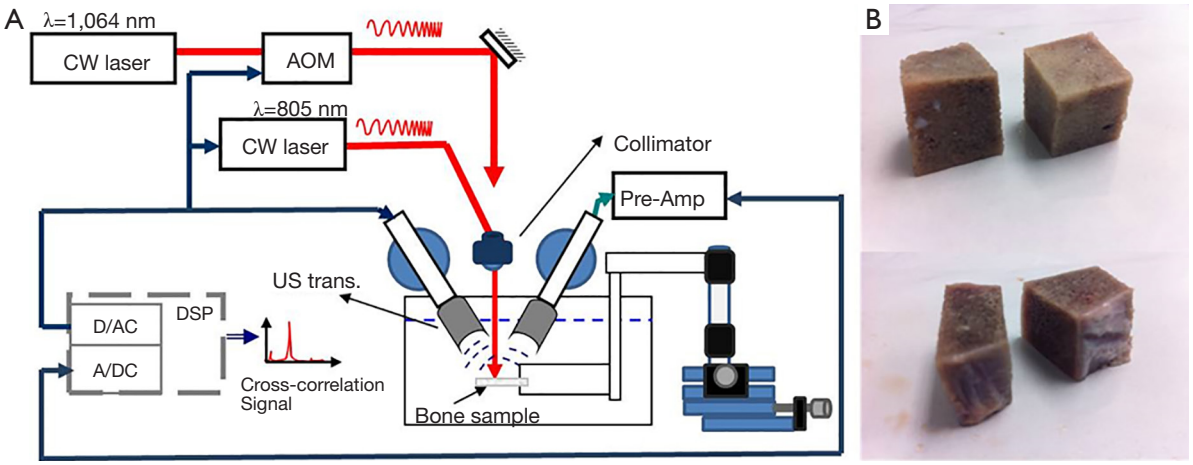

Figure 1 (A) Combined US and PA experimental set-up; (B) the first four trabecular bone samples cut from larger parts. US, ultrasound; PA, photoacoustic.

intensity. A collimator was used to generate a collimated laser beam with 2-mm spot size on the sample. There was a ~27° angle between the laser beam and each transducer center line. The direction of incidence of the laser beam was perpendicular to the water surface. The laser beam was used to adjust the focal point of both transducers on the same spot on the sample. The employed laser power was 2 W and the total laser exposure for each point measurement consisted of 10 exposures of 8 ms each with ~1 s interval between exposures.

Measurements on four samples were also performed with a CW Ytterbium laser (IPG Photonics, Oxford, MA, USA) emitting at 1,064 nm. This was done to assess the relative sensitivity of the two laser excitation wavelengths to demineralization and decollagenization of bones. To modulate the intensity of this laser, an acousto-optic modulator (Neos Technologies, Melbourn, FL, USA) was employed which was driven by signals from a function generator (AOM in *Figure 1A*). The laser power on the sample was set to 1 W, with 1-mm beam spotsize. Sample exposure was similar to the other laser. These two wavelengths were selected to maximize the penetration depth (50). Despite the large fluences, the powers of both lasers were below the maximum permissible exposure (MPE) ceiling due to the very short radiation time (51,52). Linear frequency modulation chirps and a matched filtering method were employed to generate A-scans. The chirp duration was 1 ms and A-scans were generated by averaging over 80 signal sequences. The chirp bandwidth was adjusted to maximize the PA and US SNRs. Frequency ranges used were 300 kHz to 2.6 MHz for PA, and 300 kHz to 4 MHz for US (53).

Three cattle femurs (Angus, Canadian) were purchased from a local butcher. Ten trabecular bone samples were cut from the femurs. Samples were cut with a saw to produce flat measurement areas without any cortical overlayer (*Figure 1B*). The samples were washed and kept in saline solution for up to 2 days to dissolve the blood inside the pores. The samples were treated either with ethylenediaminetetraacetic acid (EDTA) or with hypochlorite solution (NaOCl). The first group was demineralized with 50% solution of EDTA in distilled water (pH=7.7) for decalcification simulating the osteoporosis disease. This solution produces a very slow and gentle demineralization (54,55). The extent of the demineralization depends on solution concentration and exposure duration as well as on the exposed area and bone compactness. The second group was treated with sodium hypochlorite solution to decollagenize the sample (56,57). For ease of reference to the samples, those demineralized with EDTA are identified with odd numbers and the ones which were decollagenized with hypochlorite solution are classified with even numbers. The exposure duration for samples treated with EDTA was 5 hours except for sample 1 which was demineralized for 10 hours; and the samples treated with hypochlorite solution which was demineralized for 3 hours except for sample 2 which was decollegenized for 6 hours.

In one set of experiments four samples were tested with both laser wavelengths as well as with US (samples 1 to 4). These four samples were basically cut from two parts of the bone; therefore each pair had very similar properties and microstructure (*Figure 1B*). During the tests

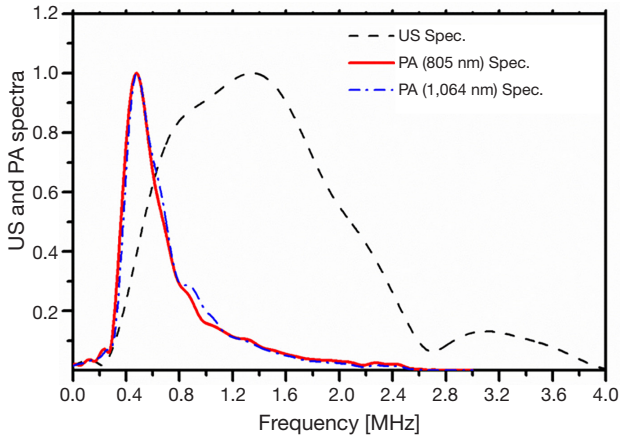

Figure 2 Spectra of US and PA reference signals. US, ultrasound; PA, photoacoustic.

the samples were fixed on a holder in the experimental set-up. Employing two micro-stages facilitated holder movement for surface scanning. The first set of US and PA experiments was performed on a ROI which included a 6×8-mm^2 rectangle on the bone sample. The evaluations consisted of 12 measurements of 3×4 points with each point 2 mm apart from the adjacent points. The samples were treated with either solution without being removed from the stage. This allowed repeating the measurements at identical locations. Afterwards, each treated sample was washed and left to dry at its location while gripped by the holder. Two hours before repeating the measurement, the tank was filled with saline solution to allow the bone to degas. This procedure helped with signal reproducibility. Comparison of PA results with both lasers showed that for the four samples under different treatment situations the 805-nm excitation exhibited slightly better depth detectability and SNR. Thus, for the remaining tests only this laser was employed. However, a complete assessment of benefits when using 1,064-nm wavelength for bone tissue characterization requires more investigation.

In the next set of experiments six bone samples were tested (samples 5 to 10). On the surface of each sample two landmarks were drilled. Also a stopper was set on the holder. The samples were screwed to a matching part that could be fixed on the holder while pushing at the stopper which controlled the height of the sample. Using the landmarks and micro-stages helped ensure the measurements could be performed at the same exact point after removing the sample for treatment and fixing it back on the holder. During the treatment, the samples were immersed in the solution and were lowered into it in a way that the two landmarks were flush with the interface, so that on one side of the bone the tissue remained intact while on the other side it was demineralized or decollagenized. US backscatter and PA back-propagating signal measurements were performed at least on 8 points at each part of the samples. These points were selected on a ROI on the surface of the bone samples and measured before and after treatments. Only the 805-nm laser was used for these samples.

All the samples were also analyzed with micro-computed tomography (μCT) as a "gold standard" for validation of our PA and US results. This process was followed before and after treatment for the first set of samples and only after treatment for the second set using μCT 40 (Scanco Medical AG, Brüttisellen, Switzerland). The μCT parameters were 40 kVp and 177 μA. To evaluate the bone volume fraction (BV/TV), the μCT analyzing software (Scano Medical) was used. Here the active volume was the aforementioned ROI on the bone with 4-mm depth/thickness.

Results

A reference signal was measured for each method to eliminate the transducer transfer function and other instrumentation components from the spectral analysis. The reference US signal was generated using a shiny metallic surface (a perfect reflector). A thick plastisol absorber with a known high absorption coefficient (9 cm^{-1} at 805 nm and ~11 cm^{-1} at 1,064 nm) was employed as the PA reference sample. The cross-correlation spectra of these reference samples are shown in *Figure 2*. The frequency spectra of PA and US signals were normalized by these spectra. In this study we used the AIB parameter defined as:

$$\text{US or PA} \quad \text{AIB}=\frac{1}{\Delta f}\int_{\Delta f} 20\log_{10}\left(\frac{S_B}{S_{ref}}\right)df \qquad [1]$$

where S_B is the amplitude spectrum of the time-gated reflected signal, S_{ref} is the amplitude spectrum from a reference sample and Δf is the frequency bandwidth of the chirp. To evaluate the US backscatter spectrum, the signal was time-gated to eliminate reflection contributions (31). However, time-gating of PA signals is not supposed to eliminate the first peak as all the signal is due to back-propagation. It should be mentioned that using a time-gating window for US that includes the reflected and backscattered US, didn't generate large variation in the results reported in *Table 1*.

The ensemble averaged US and PA cross-correlation

Table 1 Changes of US and PA (λ_1=805 nm) AIB due to demineralization and decollagenization as well as for intact bone samples (AIB and SD are calculated based on between 8 and 12 point measurements on each sample in the ROI). Also, BV/TV after the treatment in ROI.

Treatment	Sample	US AIB changes (dB)	SD	PA AIB changes (dB)	SD	BV/TV
EDTA	1	–6.1	4.6	–0.8	2.8	0.172
	3	–8.5	2.9	–7.0	2.9	0.106
	5	–5.85	2.9	–8.01	4.8	0.318
	7	–5.55	2.4	–3.28	1.9	0.150
	9	–3.70	2.7	–6.25	2.8	0.159
NaOCl	2	1.0	2.2	–13.0	2.8	0.211
	4	–1.2	2.8	–5.5	4.1	0.152
	6	3.92	2.5	–9.61	5.7	0.227
	8	1.17	2.6	–3.59	2.3	0.163
	10	5.36	3.5	–5.98	7.5	0.179
No treatment (intact part)	5	–1.46	1.9	–2.70	2.8	0.344
	6	0.42	1.6	–4.76	6.6	0.220
	7	–1.68	2.2	2.46	3.3	0.184
	8	1.83	6.4	–1.19	2.9	0.140
	9	–0.38	1.8	–0.46	4.6	0.218
	10	4.99	2.2	–2.96	4.6	0.236

US, ultrasound; PA, photoacoustic; AIB, apparent integrated backscatter/back–propagating; SD, standard deviation; ROI, regions of interest; BV/TV, bone volume fraction; EDTA, ethylenediaminetetraacetic acid; NaOCl, sodium hypochlorite solution.

signals of 12 points on sample 3 (demineralized with EDTA) are shown in *Figure 3A-C*. These signal traces demonstrate that both PA and US signals decrease after decalcification of the bone. The ensemble averaged US and PA cross-correlation signals of sample 4 (decollagenized using the sodium hypochlorite solution) are shown in *Figure 4A-C*. These signal traces demonstrate the variation of PA and US signals with decollagenization. It can be observed that the US signal shows very small variation with decollagenization, whereas PA signals at both wavelengths decreased significantly with reduction of collagen content.

To examine the consistency of the typical signals presented in *Figures 3,4* with measurements made on the other samples, the changes of the AIB values of all samples after treatments are reported in *Table 1*. Here, negative signs indicate reduction of AIB with treatment. The treated and intact parts of the samples 5-10 were also pooled together in *Table 1*. This table shows the changes in US and PA (805 nm wavelength) AIB due to different treatments; 5 demineralized samples, 5 decollagenized samples and 6 intact samples which were the intact part of samples 5 to 10. The AIB values averaged over 8 to 12 measurements on each sample and standard deviation (SD) of the changes shows value variations in each sample. The table also reports the BV/TV of the selected ROI in all cases as measured after the treatment. The small changes (compared with SD) in the AIB of the intact parts of the bones support the reproducibility of the results and define the deviation baseline of the measurement due to factors other than the treatment.

The changes in the PA AIB for the first four samples with both wavelengths are presented in *Table 2*. The BV/TV of the ROI of these four samples estimated from μCT before and after each treatment is reported in this table as well.

Table 3 shows the averaged PA (805 nm) and US AIB changes of all samples presented individually in *Table 1*. Using paired-samples Student *t*-test in an Excel program (Microsoft, USA) the statistical significance of the results was assessed and reported in the table.

US and PA AIB (λ_1=805 nm) *vs*. BV/TV were plotted in *Figure 5*. The linear least-squares fit has been used for each group separately to show trends. The linear regression (LR) of the group treated with EDTA is shown with solid lines, while the group treated with sodium hypochlorite is identified by dashed lines. The associated data points

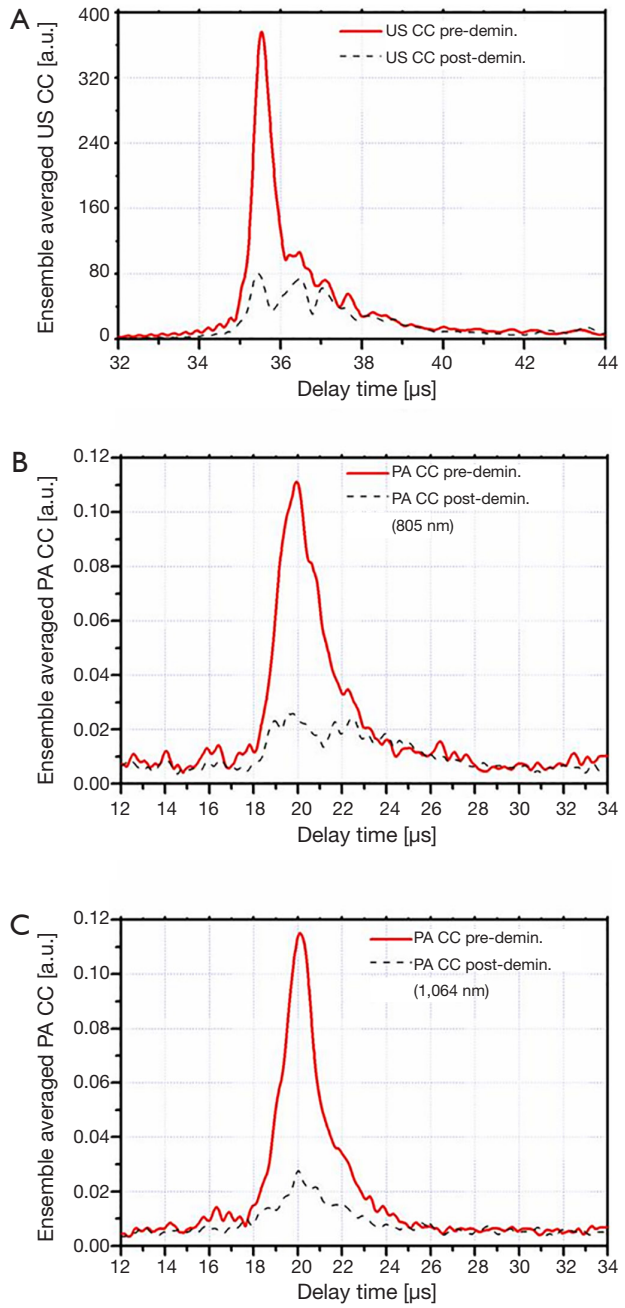

Figure 3 Ensemble averaged CC signals of sample 3 before and after demineralization. (A) US; (B) PA (λ_1=805 nm); (C) PA (λ_2=1,064 nm). CC, cross-correlation; US, ultrasound; PA, photoacoustic.

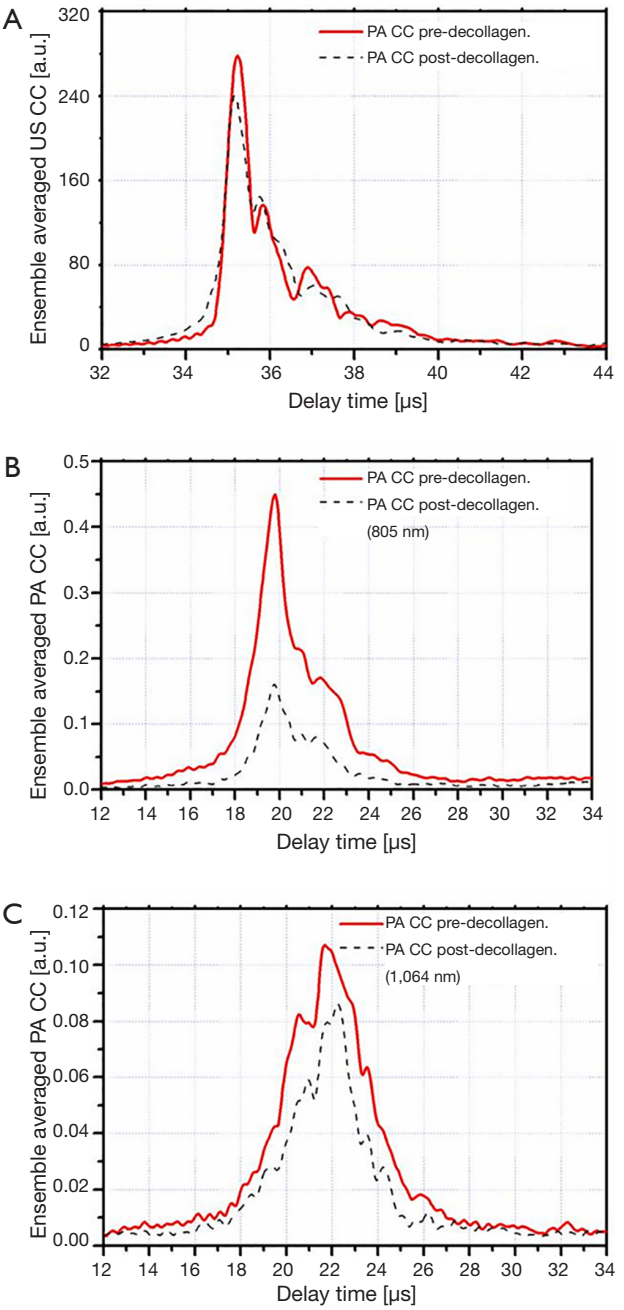

Figure 4 Ensemble averaged CC signals of sample 4 before and after decollagenization. (A) US; (B) PA (λ_1=805 nm); (C) PA (λ_2=1,064 nm). CC, cross-correlation; US, ultrasound; PA, photoacoustic.

Table 2 Comparison between the changes of PA AIB due to demineralization and decollagenization of bone samples with two different laser wavelengths (AIB and SD are calculated based on between 12 point measurements on each sample in ROI). Also, BV/TV of samples before and after treatment.

Treatment	Sample	PA AIB change (805 nm) (dB)	SD	PA AIB change (1,064 nm) (dB)	SD	BV/TV before	BV/TV after
EDTA	1	–0.8	2.8	+1.0	2.4	0.229	0.172
	3	–7.0	2.9	–6.3	3.1	0.117	0.106
NaOCl	2	–13.0	2.8	–13.9	1.7	0.234	0.211
	4	–5.5	4.1	–3.4	4.5	0.159	0.152

PA, photoacoustic; AIB, apparent integrated backscatter/back-propagating; SD, standard deviation; ROI, regions of interest; BV/TV, bone volume fraction; EDTA, ethylenediaminetetraacetic acid; NaOCl, sodium hypochlorite solution.

Table 3 Averaged changes of US and PA (λ_1=805 nm) AIB of sample bones demineralized, decollagenized, or intact

Treatment	No. of samples	US AIB change (dB)	PA AIB change (dB)
EDTA	5	–5.94**	–5.07*
NaOCl	5	2.05	–7.53*
No treatment	6	0.62	–1.60

**, statistically significant with 99% confidence (P<0.01); *, statistically significant with 97.5% confidence (P<0.025). US, ultrasound; PA, photoacoustic; AIB, apparent integrated backscatter/back-propagating; EDTA, ethylenediaminetetraacetic acid; NaOCl, sodium hypochlorite solution.

are also shown with solid symbols and half-filled symbols, respectively.

Discussion

The use of combined US and PA probes in parallel is expected to enhance the detection of bone degradation. While for the most part both methods use common instrumentation, they are sensitive to different tissue properties. The key goal of this study was to explore the PA and US responses before and after decalcification and decollagenization of the bone samples at identical points. The measurement methodology used helps to reduce the effect of the large disparity and inhomogeneity of the bone tissue on experimental results. Different regions of the

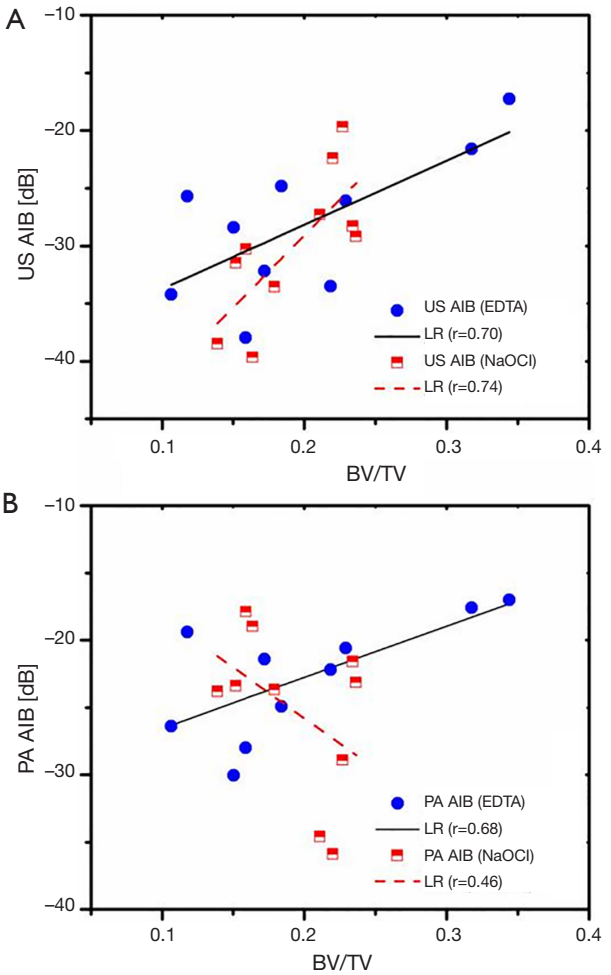

Figure 5 (A) US and (B) PA (λ_1=805 nm) apparent integrated backscatter/back-propagating (AIB) versus bone volume fraction (BV/TV). US, ultrasound; PA, photoacoustic.

samples were treated with EDTA and sodium hypochlorite solutions. The former dissolves the minerals and the latter reduces the collagen content. These experiments were designed to evaluate the relative sensitivity of the two modalities to trabecular bone degradation. The cross-correlation signal traces shown in *Figure 3A-C* as well as *Figure 4A-C* are averaged from 12 point measurements which did not demonstrate large signal fluctuations. Comparison between the FWHM of US and PA signals demonstrates the higher axial resolution of US compared with PA, although both modalities used the same detector. The chirp frequency ranges of the two methods were somewhat different: 0.3-2.6 MHz for PA *vs*. 0.3-4 MHz for US. Nevertheless, this difference has little to do with resolution differences, as it is mostly the effect of PA energy conversion which acts as a low-pass filter (53,58). *Figure 2* shows the PA and US reference spectra and clearly demonstrates a much broader US frequency range compared to PA. It also clarifies the rationale for choosing a shorter frequency range for PA compared with US.

The cross-correlation signals of both methods (PA and US) show decrease with decalcification of the bone samples. US AIB as well as PA AIB with 805-nm laser show decrease for all five samples. However, PA measurements with the 1,064-nm laser have one exception to the trend: sample 1. It should be noticed that in this case the change with respect to SD was small. This discrepancy can be explained by considering that minerals absorb and scatter the laser light. The decalcification process reduces these absorbers (PA sources) and at the same time reduces scattering, thereby facilitating the penetration of light into deeper subsurface regions which might have higher absorption coefficients. The reason that this only happened for one sample can be related to normal variation in biological samples. It should be noticed that the change of PA AIB at 805 nm in this case has a negative value and it is small compared with its SD, therefore insignificant.

Table 1 shows that the reduction of collagen content increases the US AIB. Here the acoustic-wave-attenuating collagen is reduced and the US signal is consequently increased. Sample 4 is an exception in the sense that its US AIB decreased with decollagenization. On the other hand, it can be observed that the average change of the US AIB is smaller than the SD, and therefore insignificant. This can also be observed in *Figure 4A* where the ensemble averaged cross-correlation of US measurements on sample 4 is shown.

Table 1 further shows that the PA AIB decreased for all decollagenized samples. This is also the case for the other wavelength (1,064 nm) in *Table 2*. Therefore, as discussed in relation to *Figure 4*, we consistently observed PA-signal and consequently PA AIB decrease with reduction of bone collagen content.

The variation of AIB with BV/TV in the demineralized cases (*Figure 5A*,*B* solid lines) demonstrates the sensitivity of both US and PA to changes in the mineral content in the ROI. In *Figure 5B*, however, it can be seen that in the case of treatment with sodium hypochlorite (dashed line), the trend of PA AIB does not follow the reduction in BV/TV (negative slope). This is not surprising as this group has lost the collagen content without significant variation of the BV/TV. Thus, the changes in PA AIB were completely affected by decollagenization. In contrast, *Figure 5A* (dashed line) shows that for the same group (decollagenized samples), the US AIB follows the trend of BV/TV change but with a slope change compared to demineralized samples. This indicates that US AIB has a strong correlation with BV/TV and decollagenization induces a minor variation in this correlation, which is consistent with the results discussed in relation with *Table 1*. We observed a slight (compared with SD) increase of US AIB with decollagenization which was attributed to reduction in acoustic attenuation and, therefore, we should expect higher correlation of backscattering with BV/TV. This is the case in *Figure 5A* where the correlation coefficient between US AIB and BV/TV, increased from 0.7 to 0.74 for decollagenized samples. It should be noted that despite strong correlation of US with BV/TV, the QUS parameters, especially the backscatter parameters, are affected by other factors such as the random structure and anisotropy of cancellous bone. Although one may use a very large number of samples to minimize the influence of those other factors in the study, our approach was to perform the measurements exactly at the same points before and after all treatments. Thus, other parameters generate a fixed baseline and treatment-induced changes to this baseline can be easily monitored.

The results of this study are summarized in *Table 3*, which shows the average change of US and PA AIB, before and after the measurements from three groups of samples: demineralized samples (identified with EDTA treatment), decollagenized samples (identified with NaOCl) and intact samples (identified with "no treatment"). The number of samples for the first two groups was 5 and for the intact group was 6. As mentioned before, the data for the intact samples were from the untreated part of samples 5 to 10. Using the paired *t*-test the statistical significance of the changes was analyzed. Considering the samples treated with

sodium hypochlorite, while the US AIB was not significantly sensitive to the changes, the PA AIB is sensitive and could detect the variation in collagen content. These conclusions are consistent with the ensemble averaged cross-correlation signals of samples 3 and 4 shown in *Figure 3* and *Figure 4*, respectively. On the contrary, for samples treated with EDTA, both US and PA are statistically significant and could detect the changes in BV/TV. However, the US AIB seems to be more reliable than PA as indicated by the P values reported in *Table 3*.

In conclusion, in this study we examined the variation of US backscatter and PA back-propagation with reduction of bone minerals and collagen content in trabecular bones. The results show that both PA and US are sensitive to reduction of the mineral content of bone. Moreover, PA is also sensitive to changes in the collagen content of bone, but US is not significantly sensitive to these changes. The PA response depends on the optical properties of tissue, thus it is expected to provide QUS (the US clinical embodiment) with complementary information about bone health and integrity. In addition, it requires minimum effort for co-registration with US. This can elevate the combined method to a collagen specific diagnostic, capable of analyzing the optical and mechanical properties of bone tissue. While the collagen status is directly related to the strength of the bone (3,4,59) diagnosis of its condition with QUS is a challenge (27,33,56). Here it has been shown that the back-propagating PA has a great advantage over US backscattering measurements with respect to collagen variation sensitivity. The combined method can yield information about changes to trabecular bone density with respect to both mineral and collagen content, which is not possible with US probing alone.

Acknowledgements

The authors gratefully acknowledge the support of the Canada Research Chairs program, the NSERC Discovery Grants program, and the Canada Council for the Arts through a Killam Fellowship to A.M. The authors acknowledge the help of Professor J. E. Davis and Dr. Elnaz Ajami (IBBME, University of Toronto) in performing the μCT of the bone samples.

Authors' contributions: The overall study was designed by AM with contribution from BL. The experimental set-up and software were implemented by BL. Both BL and LY contributed in the preparation of the samples and performed the experiments. Data analysis and drafting of the paper were performed by BL and AM. AM contributed to the analysis and interpretation of the data, revisions of the article, the discussion and the conclusions.

Disclaimer: Since there is no live animal involved in this research, no animal use protocol approval was required from the Office of Research Ethics, University of Toronto.

References

1. Fogelman I, Blake GM. Different approaches to bone densitometry. J Nucl Med 2000;41:2015-25.
2. Ritchie RO, Buehler MJ, Hansma P. Plasticity and Toughness in Bone. Physics Today 2009;62:41-7.
3. Launey ME, Buehler MJ, Ritchie RO. On the Mechanistic Origins of Toughness in Bone. J Mater 2010;40:25-53.
4. Viguet-Carrin S, Garnero P, Delmas PD. The role of collagen in bone strength. Osteoporos Int 2006;17:319-36.
5. Bailey AJ, Sims TJ, Ebbesen EN, Mansell JP, Thomsen JS, Mosekilde L. Age-related changes in the biochemical properties of human cancellous bone collagen: relationship to bone strength. Calcif Tissue Int 1999;65:203-10.
6. Wang X, Shen X, Li X, Agrawal CM. Age-related changes in the collagen network and toughness of bone. Bone 2002;31:1-7.
7. Leeming DJ, Henriksen K, Byrjalsen I, Qvist P, Madsen SH, Garnero P, Karsdal MA. Is bone quality associated with collagen age? Osteoporos Int 2009;20:1461-70.
8. Saito M, Marumo K. Collagen cross-links as a determinant of bone quality: a possible explanation for bone fragility in aging, osteoporosis, and diabetes mellitus. Osteoporos Int 2010;21:195-214.
9. Wang X, Bank RA, TeKoppele JM, Agrawal CM. The role of collagen in determining bone mechanical properties. J Orthop Res 2001;19:1021-6.
10. Knott L, Whitehead CC, Fleming RH, Bailey AJ. Biochemical changes in the collagenous matrix of osteoporotic avian bone. Biochem J 1995;310:1045-51.
11. Langton CM, Palmer SB, Porter RW. The measurement of broadband ultrasonic attenuation in cancellous bone. Eng Med 1984;13:89-91.
12. Njeh CF, Boivin CM, Langton CM. The role of ultrasound in the assessment of osteoporosis: a review. Osteoporos Int 1997;7:7-22.
13. Langton CM, Njeh CF. The measurement of broadband ultrasonic attenuation in cancellous bone--a review of the science and technology. IEEE Trans Ultrason Ferroelectr

Freq Control 2008;55:1546-54.
14. Laugier P. Instrumentation for in vivo ultrasonic characterization of bone strength. IEEE Trans Ultrason Ferroelectr Freq Control 2008;55:1179-96.
15. Laugier P, Haiat G. Bone quantitative ultrasound, Springer Dordrecht Heidelberg London New York: Science+Business Media BV 2011;409-40.
16. Mano I, Horii K, Takai S, Suzaki T, Nagaoka H, Otani T. Development of novel ul-trasonic bone densitometry using acoustic properties of cancellous bone for fast and slow waves. Jpn J Appl Phys 2006;45:4700-2.
17. Wear KA. Ultrasonic scattering from cancellous bone: a review. IEEE Trans Ultrason Ferroelectr Freq Control 2008;55:1432-41.
18. Litniewski J, Cieslik L, Lewandowski M, Tymkiewicz R, Zienkiewicz B, Nowicki A. Ultrasonic scanner for in vivo measurement of cancellous bone properties from backscattered data. IEEE Trans Ultrason Ferroelectr Freq Control 2012;59:1470-7.
19. Wear KA. Frequency dependence of ultrasonic backscatter from human trabecular bone: theory and experiment. J Acoust Soc Am 1999;106:3659-64.
20. Nicholson PH, Strelitzki R, Cleveland RO, Bouxsein ML. Scattering of ultrasound in cancellous bone: predictions from a theoretical model. J Biomech 2000;33:503-6.
21. Jenson F, Padilla F, Laugier P. Prediction of frequency-dependent ultrasonic backscatter in cancellous bone using statistical weak scattering model. Ultrasound Med Biol 2003;29:455-64.
22. Chaffaï S, Roberjot V, Peyrin F, Berger G, Laugier P. Frequency dependence of ultrasonic backscattering in cancellous bone: autocorrelation model and experimental results. J Acoust Soc Am 2000;108:2403-11.
23. Wear KA, Garra BS. Assessment of bone density using ultrasonic backscatter. Ultrasound Med Biol 1998;24:689-95.
24. Wear KA, Armstrong DW. The relationship between ultrasonic backscatter and bone mineral density in human calcaneus. IEEE Trans Ultrason Ferroelectr Freq Control 2000;47:777-80.
25. Ta D, Wang W, Huang K, Wang Y, Le LH. Analysis of frequency dependence of ultrasonic backscatter coefficient in cancellous bone. J Acoust Soc Am 2008;124:4083-90.
26. Il Lee K, Joo Choi M. Frequency-dependent attenuation and backscatter coefficients in bovine trabecular bone from 0.2 to 1.2 MHz. J Acoust Soc Am 2012;131:EL67-73.
27. Karjalainen JP, Töyräs J, Riekkinen O, Hakulinen M, Jurvelin JS. Ultrasound backscatter imaging provides frequency-dependent information on structure, composition and mechanical properties of human trabecular bone. Ultrasound Med Biol 2009;35:1376-84.
28. Riekkinen O, Hakulinen MA, Töyräs J, Jurvelin JS. Spatial variation of acoustic properties is related with mechanical properties of trabecular bone. Phys Med Biol 2007;52:6961-8.
29. Hoffmeister BK, Jones CI 3rd, Caldwell GJ, Kaste SC. Ultrasonic characterization of cancellous bone using apparent integrated backscatter. Phys Med Biol 2006;51:2715-27.
30. Hoffmeister BK, Johnson DP, Janeski JA, Keedy DA, Steinert BW, Viano AM, Kaste SC. Ultrasonic characterization of human cancellous bone in vitro using three different apparent backscatter parameters in the frequency range 0.6-15.0 mhz. IEEE Trans Ultrason Ferroelectr Freq Control 2008;55:1442-52.
31. Hoffmeister BK. Frequency dependence of apparent ultrasonic backscatter from human cancellous bone. Phys Med Biol 2011;56:667-83.
32. Hakulinen MA, Day JS, Töyräs J, Weinans H, Jurvelin JS. Ultrasonic characterization of human trabecular bone microstructure. Phys Med Biol 2006;51:1633-48.
33. Riekkinen O, Hakulinen MA, Lammi MJ, Jurvelin JS, Kallioniemi A, Töyräs J. Acoustic properties of trabecular bone--relationships to tissue composition. Ultrasound Med Biol 2007;33:1438-44.
34. Hakulinen MA, Töyräs J, Saarakkala S, Hirvonen J, Kröger H, Jurvelin JS. Ability of ultrasound backscattering to predict mechanical properties of bovine trabecular bone. Ultrasound Med Biol 2004;30:919-27.
35. Roux C, Roberjot V, Porcher R, Kolta S, Dougados M, Laugier P. Ultrasonic backscatter and transmission parameters at the os calcis in postmenopausal osteoporosis. J Bone Miner Res 2001;16:1353-62.
36. Lashkari B, Mandelis A. Combined photoacoustic and ultrasonic diagnosis of early bone loss and density variations. Proc SPIE 8207, Photonic Therapeutics and Diagnostics VIII, 82076K (February 3, 2012).
37. Lashkari B, Mandelis A. Photoacoustic and ultrasonic signatures of early bone density variations, Proc SPIE Society of Photo-Optical Instrumentation Engineering, Conf. 8565 ("Photonic Therapeutics and Diagnostics IX"), San Francisco, USA, 2013;8565:85656I1-10, SPIE Press, April, 2013.
38. Lashkari B, Mandelis A. Coregistered photoacoustic and ultrasonic signatures of early bone density variations. J Biomed Opt 2014;19:36015.

39. Yang L, Lashkari B, Mandelis A, Tan JW. Bone Composition Diagnostics: Photoacoustics Versus Ultrasound. Int J Thermophys 2014. [Epub ahead of print]. doi: 10.1007/s10765-014-1701-6
40. Steinberg I, Eyal A, Gannot I. Multispectral photoacoustic method for the early detection and diagnosis of osteoporosis. Proc SPIE 8565, Photonic Therapeutics and Diagnostics IX, 85656G (8 March 2013).
41. Zhao Z, Moilanen P, Karppinen P, Määttä M, Karppinen T, Hæggström E, Timonen J, Myllylä R. Photo-acoustic excitation and detection of guided ultrasonic waves in bone samples covered by a soft coating layer. Proc SPIE 8553, Optics in Health Care and Biomedical Optics V, 85531E (December 11, 2012).
42. Nowicki A, Litniewski J, Secomski W, Lewin PA, Trots I. Estimation of ultrasonic attenuation in a bone using coded excitation. Ultrasonics 2003;41:615-21.
43. Lin W, Xia Y, Qin YX. Characterization of the trabecular bone structure using frequency modulated ultrasound pulse. J Acoust Soc Am 2009;125:4071-7.
44. Lashkari B, Manbachi A, Mandelis A, Cobbold RS. Slow and fast ultrasonic wave detection improvement in human trabecular bones using Golay code modulation. J Acoust Soc Am 2012;132:EL222-8.
45. Song X, Ta D, Wang W. A base-sequence-modulated Golay code improves the excitation and measurement of ultrasonic guided waves in long bones. IEEE Trans Ultrason Ferroelectr Freq Control 2012;59:2580-3.
46. Fan Y, Mandelis A, Spirou G, Vitkin IA. Development of a laser photothermoacoustic frequency-swept system for subsurface imaging: theory and experiment. J Acoust Soc Am 2004;116:3523-33.
47. Telenkov SA, Mandelis A. Fourier-domain biophotoacoustic subsurface depth selective amplitude and phase imaging of turbid phantoms and biological tissue. J Biomed Opt 2006;11:044006.
48. Telenkov SA, Mandelis A, Lashkari B, Forcht M. Frequency-domain photothermoacoustics: Alternative imaging modality of biological tissues. J Appl Phys 2009;105:102029-8.
49. Panametrics. NDT Ultrasonic Transducers for Nondestructive Testing 2010. Available online: http://www.olympus-ims.com/data/File/panametrics/panametrics-UT.en.pdf
50. Genina EA, Bashkatov AN, Tuchin VV. Optical Clearing of Cranial Bone. Adv Optical Technologies 2008;267867.
51. American National Standard for the Safe Use of Lasers. Standard Z136.1-2007. ANSI Inc. New York: 2007.
52. Lashkari B, Mandelis A. Comparison between pulsed laser and frequency-domain photoacoustic modalities: signal-to-noise ratio, contrast, resolution, and maximum depth detectivity. Rev Sci Instrum 2011;82:094903.
53. Lashkari B, Mandelis A. Linear frequency modulation photoacoustic radar: optimal bandwidth and signal-to-noise ratio for frequency-domain imaging of turbid media. J Acoust Soc Am 2011;130:1313-24.
54. Callis G, Sterchi D. Decalcification of Bone Literature Review and Practical Study of Various Decalcifying Agents Methods and Their Effect on Bone Histology. J Histotechnol 1998;21:49-58.
55. Ehrlich H, Koutsoukos PG, Demadis KD, Pokrovsky OS. Principles of demineralization: modern strategies for the isolation of organic frameworks. Part II. Decalcification. Micron 2009;40:169-93.
56. Hoffmeister BK, Whitten SA, Kaste SC, Rho JY. Effect of collagen and mineral content on the high-frequency ultrasonic properties of human cancellous bone. Osteoporos Int 2002;13:26-32.
57. Langton CM. Osteoporosis: case of skeletal biocorrosion. Corrosion Engineering, Science and Technology 2007;42:339-343.
58. Lashkari B, Mandelis A. Photoacoustic radar imaging signal-to-noise ratio, contrast, and resolution enhancement using nonlinear chirp modulation. Opt Lett 2010;35:1623-5.
59. Wynnyckyj C, Willett TL, Omelon S, Wang J, Wang Z, Grynpas MD. Changes in bone fatigue resistance due to collagen degradation. J Orthop Res 2011;29:197-203.

Cite this article as: Lashkari B, Yang L, Mandelis A. The application of backscattered ultrasound and photoacoustic signals for assessment of bone collagen and mineral contents. Quant Imaging Med Surg 2015;5(1):46-56. doi: 10.3978/j.issn.2223-4292.2014.11.11

